Marine Geology 492 (2026) 107694

Contents lists available at ScienceDirect

Marine Geology

journal homepage: www.elsevier.com/locate/margo

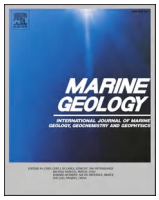

Anthropogenic disturbances drive stepwise geomorphic changes of shoal-channel systems in a tide-dominated estuary

Ping Zhang [a], Linxi Fu [b], Xiangyuan Li [b], Jianliang Lin [b], Huayang Cai [b], Zhijun Dai [a,*], Qingshu Yang [b,*]

[a] State Key Laboratory of Estuarine and Coastal Research, East China Normal University, Shanghai 200241, China
[b] School of Ocean Engineering and Technology, Sun Yat-Sen University, Zhuhai 519082, China

ARTICLE INFO

Editor: N Senechal

Keywords:
Shoal-channel system
Deposition and erosion
Anthropogenic disturbances
Tide-dominant estuary
Shiziyang Tidal Channel

ABSTRACT

The shoal-channel system, a fundamental geomorphic feature in estuaries globally, plays a crucial role in ensuring navigational safety and sustaining estuarine-deltaic ecosystem services. However, in the Anthropocene, this system has undergone significant transformations, challenging its stability and functional integrity. To investigate these changes, we applied a Digital Elevation Model (DEM) and Morphological Shannon Entropy (MSE) to quantify the stepwise evolution of the shoal-channel system in the Shiziyang (SZY) Tidal Channel, a tide-dominated reach of the Pearl River Estuary (PRE). Our findings reveal that anthropogenic disturbances triggered a systematic eastward channel migration, progressive shoal expansion, and peak erosion of 2.37×10^6 m^3/yr during Period III (1989–2000), exceeding concurrent deposition by 50 %. These changes culminated in a systemic reconfiguration from a V-shaped to a W-shaped channel profile. Sequential dredging emerged as the principal driver, accounting for a 17 m incision and contributing up to 68.45 % of the total scouring in Period III. Additional factors, including port construction (which reduced channel width by 20.39 %), diminished sediment flux (causing a 27.65 % decrease in depositional bank extent), and intensified hydrodynamics (reflected by a tidal range increase of 4.56 mm/yr), acted synergistically to amplify the regime shift. By elucidating the key drivers and consequences of this geomorphic evolution, our study provides critical insights for the sustainable management of heavily engineered coastal systems in the Anthropocene.

1. Introduction

Shoal-channel systems, which are fundamental geomorphic units in estuaries worldwide (Barua, 1990; Lou et al., 2020) including river deltas and coastal embayments, serve as essential navigation corridors and natural coastal defense buffers. These systems exhibit distinct meandering configurations, comprising flood- and ebb-dominated channels separated by intertidal shoals. The morphodynamic evolution of shoal-channel systems is governed by the interplay of fluvial discharge (Xie et al., 2022), tidal forcing (Moore et al., 2009), wave energy (Pratolongo et al., 2010), and their nonlinear interactions (Caldwell et al., 2019; Dyer, 1977; Galloway, 1975). Sediment transport dynamics are particularly significant, with shoals facilitating seaward sediment dispersal while channels promote landward sediment transfer (Zhou et al., 2021; Yang et al., 2025; Wang et al., 2025). Distinctively, morphodynamics in tide-dominant estuaries are intrinsically linked to tidal-fluvial interactions, as exemplified by the Ganges-Brahmaputra-Meghna (Barua, 1990), Hangzhou Bay (Xie et al., 2022), and Amazon Estuary (Abad et al., 2025).

Under steady forcing conditions, estuarine channel-shoal systems exhibit dynamic equilibrium or quasiperiodic behavior as intrinsic characteristics (Kleinhans et al., 2015; Hoitink et al., 2020; Chan et al., 2024). The stability of these systems holds critical importance for flood mitigation, freshwater resource management, navigational safety, land availability, biodiversity habitats, and broader estuarine-deltaic ecosystem services (Syvitski and Saito, 2007). However, both extreme events (Bilskie et al., 2016; Kuang et al., 2020; Röbke et al., 2025) and anthropogenic disturbances (Huang et al., 2023; Wang et al., 2024) have significantly altered sedimentation-hydrodynamics-morphology feedback in natural shoal-channel systems. Furthermore, intensified human interventions in recent decades have driven pronounced reorganization of channel-shoal configurations globally (Dai, 2021; Van Maren et al., 2023a, 2023b; Zhong et al., 2024; Schrijvershof et al., 2024), highlighting the urgent need for a mechanistic understanding of these

* Corresponding authors.
E-mail addresses: zjdai@sklec.ecnu.edu.cn (Z. Dai), yangqsh@mail.sysu.edu.cn (Q. Yang).

https://doi.org/10.1016/j.margeo.2025.107694
Received 23 October 2025; Accepted 6 December 2025
Available online 8 December 2025

anthropogenic impacts to inform sustainable management frameworks.

These transformations of the shoal-channel system are particularly evident in the shoal-channel system's significant evolution during the Anthropocene (Lou et al., 2018, 2020; Zeng et al., 2024), where direct bathymetric alterations from channel dredging and sand mining have emerged as dominant forcing factors (Zeng et al., 2024; Jia et al., 2024; Röbke et al., 2025). Moreover, its morphology has been further modified by land reclamation and port development, intensifying hydrodynamic conditions (Talke and Jay, 2020; Van Maren et al., 2023b; Zhong et al., 2024; Schrijvershof et al., 2024; Zhang et al., 2025a, 2025b). Dam construction has fundamentally altered sediment regimes (Colina Alonso et al., 2021; Yang et al., 2025), resulting in sediment reductions of more than 50 % in globally analogous systems. These reductions have triggered shoal degradation in major deltas such as the Mississippi and Yangtze, while significantly increasing channel maintenance costs in estuarine systems like Chesapeake Bay. In addition, decadal-scale processes (Shimozono et al., 2019) and morphodynamic lag relative to sea-level rise (Konyssova et al., 2025; Röbke et al., 2025) further complicate system response, altering tidal asymmetry and sediment budgets. While existing studies have elucidated the impacts of anthropogenic activities on shoal-channel systems generally, the specific evolutionary trajectory of the Shiziyang (SZY) Tidal Channel system under combined river modifications and engineering interventions remains underexplored.

With a length of around 30 km, the SZY tide-dominant Tidal Channel is located on the eastern flank of the Pearl River Estuary (PRE) (Fig. 1b). The tidal characteristics of the Shiziyang Tidal Channel are irregular semi-diurnal tidal types, with an average tidal range of about 1.06–1.69 m. A spatial gradient in tidal dynamics is observed along the SZY, transitioning from ebb-dominance in the lower reach ($\gamma_N = -0.008$ at Sishengwei) to flood-dominance in the upper reach ($\gamma_N = +0.064$ at Huangpu), reflecting systematic along-channel variations in tidal asymmetry (Lin et al., 2025). The SZY Tidal Channel receives all the water from the Liuxi River and the East River network, collects about 60 % of the runoff from the North River, and flows southward into the South China Sea. The average annual runoff is 5.86×10^{10} m^3, accounting for about 19 % of the total runoff in the Pearl River Basin (PRB). The average yearly sediment transport of the tidal channel is 8.85×10^7 t/yr, accounting for 10 % of the total sediment transport in the PRB. Human interventions have significantly altered the morphodynamic processes in the Pearl River Estuary, including channel dredging in Lingding Bay (Cai et al., 2012; Chen et al., 2022; Chu et al., 2022; Wang et al., 2020), extensive sand mining across the Pearl River network, and large-scale dam construction within the basin. Nevertheless, the mechanistic linkages between these anthropogenic forcings and the morphological evolution of the shoal-channel system in the SZY tidal channel remain inadequately constrained.

Therefore, understanding the morphological responses of channels and shoals to anthropogenic intervention is a key issue for coastal protection and management. In this study, we focus on the morphological evolution of the shoal-channel system in SZY Tidal Channel, with the following key objectives: (1) to investigate recent decadal variations in the SZY; (2) to identify its morphodynamic patterns; and (3) to assess the potential impacts of natural and anthropogenic forcing mechanisms on SZY evolution.

2. Materials and methods

2.1. Datasets

The morphological evolution of the SZY Tidal Channel was analyzed using six datasets (from 1955, 1979, 1989, 2000, 2010, and 2019), all referenced to the Lowest Astronomical Tide Datum. Detailed data sources and specifications are compiled in Table S1 (*Supplementary materials*) To evaluate the reliability of multi-source historical chart data, a unified error propagation model was systematically applied to estimate the root mean square error (RMSE) of tidal level normalization for each dataset. The composite formula of the model is as follows:

$$RMSE_{tide} = \sqrt{(E_{time})^2 + (\Delta H)^2} \quad (1)$$

where $RMSE_{tide}$ represents the total RMSE of tidal level normalization and serves as the core evaluation metric; E_{time} is the vertical error component caused by time synchronization error Δt, calculated as $E_{time} = V_{max} \times \Delta t$; ΔH is the tidal height interpolation error, uniformly set to ±0.25 m based on the technological level of historical data; Δt is the time synchronization error, uniformly set to ±30 min, considering the

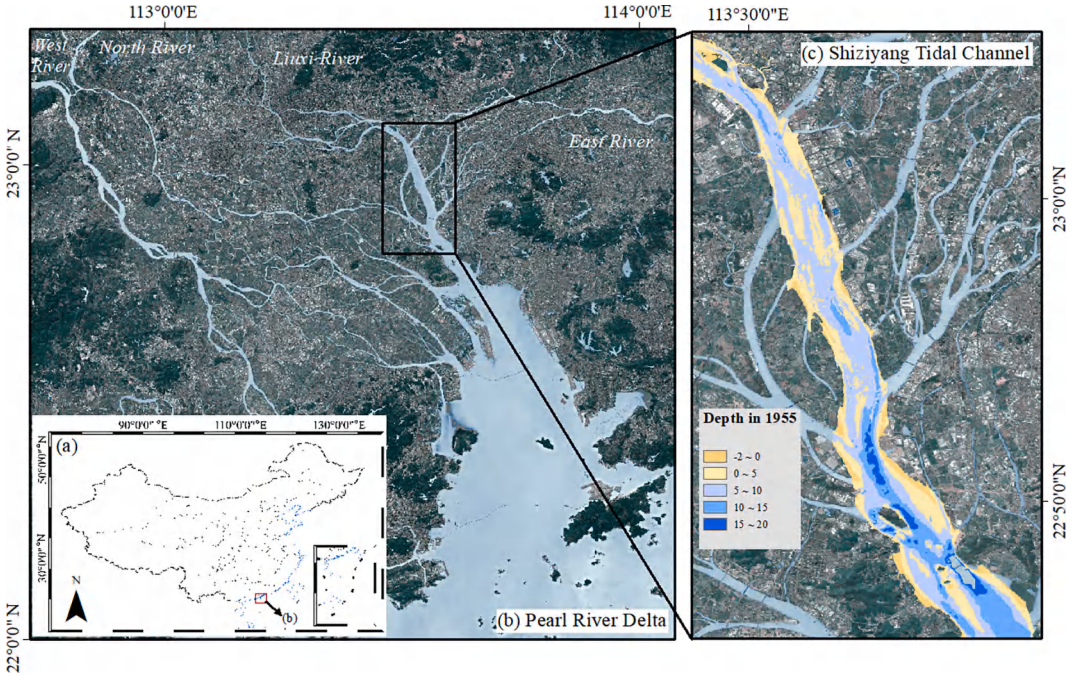

Fig. 1. Overview of the PRD (a) and SZY Tidal Channel (b).

timing and positioning accuracy of historical measurements; V_{max} is the maximum tidal change rate, estimated using $V_{max} = k \times V_{mean}$, where V_{mean} is the average tidal change rate, derived from the tidal range R in the tidal information table and the semi-tidal period $T_{1/2}$, i.e., $V_{mean} = R/T_{1/2}$, and k is an empirical amplification factor, set to 1.5 to conservatively estimate the maximum change rate.

The results (see Table S2 in the *Supplementary Materials*) show that the tidal level normalization errors of the twelve datasets in this study range from ±0.30 m to ±0.46 m. The error magnitude is highly positively correlated with the tidal range of the survey area: for stations with a tidal range R of approximately 1.5 m, the error stabilizes at around ±0.30 m, while the station with the largest tidal range, Nizhoutou (R = 3.1 *m*), also has the largest error ($RMSE_{tide}$ = ±0.46 m). Based on this evaluation, we regard ±0.30 m as the typical tidal level normalization error for this study area under an average tidal range (approximately 1.5 m). Therefore, in subsequent analyses, when topographic changes of less than 0.5 m (particularly less than 0.3 m) are observed, they will be treated with caution, and such data will not be included in the final statistical results to ensure the reliability of the conclusions.

In addition, daily high and low water level time series (1965–2017) from two gauging stations were collected, including Sishengwei (denoted by SSW) and Huangpu (denoted by HP), and their locations are shown in the *Supplementary Materials*. Here, the water level time series in SSW and HP stations were collected from the hydrological data of the PRB. Water level data were standardized to the Pearl River Datum and interpolated to hourly values employing a trigonometric interpolation technique (Zhang et al., 2018). The high consistency between observed and interpolated values, as shown in Fig. S1 (*Supplementary Materials*), validates the reliability of this preprocessing step.

2.2. Bathymetric data processing methods

The Digital Elevation Model (DEM) of SZY was generated, and the bathymetric data were converted from the local lowest tidal level to the Pearl River Datum. Projected to UTM-WGS84 coordinates of China, the data were interpolated to a 20 m × 20 m grid DEM in the ArcGIS software. For pre-1970s single-beam sonar data, characterized by sparse survey lines, an interpolation RMSE of ±2.0 m was estimated using the basic contour interval of adjacent land topography as a proxy for overall survey quality. In contrast, for post-1970s multi-beam sonar data, the high-density swath coverage rendered the errors associated with grid interpolation negligible.

Based on the extracted DEM, the bulk geometry can be described by the exponential functions of the tidally averaged cross-sectional area $\bar{A}$ and width $\bar{B}$:

$$\overline{A} = \overline{A_0}\exp(-x/a) \tag{2}$$

$$\overline{B} = \overline{B_0}\exp(-x/b) \tag{3}$$

where x is the longitudinal coordinate directed landward; $\bar{A}_0$ and $\bar{B}_0$ represent values at the estuary mouth; a and b are the convergence lengths of the cross-sectional area and width, respectively.

2.3. Morphological Shannon Entropy (MSE)

Morphology Shannon Entropy can be used as the phenomenological state function of the system morphodynamic equilibrium (Wu et al., 2018; Fu et al., 2025). Here, the Shannon Entropy $H(X)$ of a discrete system can be defined as the statistical means of the probability of a random event:

$$H(X) = -\sum_{i=1}^{n} P(x_i)\log_2 P(x_i) \tag{4}$$

where X is the set of random events x_i; $P(x_i)$ is the probability of random events x_i, and the probability space of random variables is:

$$\begin{bmatrix} X \\ P \end{bmatrix} = \begin{bmatrix} x_1, & x_2, & \ldots & x_n \\ P(x_1), & P(x_2), & \ldots, & P(x_n) \end{bmatrix} \tag{5}$$

Where n is the total number of bins to discretize. The Shannon Entropy indicates the average uncertainty of the event and quantifies the average level of information contained in the messages.

In the Morphology Shannon Entropy (MSE), x_i is the depth h_i in the system, $P(xi)$ is the percentage of water area corresponding to the depth h_i, and n is the number of water depth classifications. In this study, we set $n = 40$ when the water depth range is 0–30 m after justifying the number of depth bins (See Fig.S2-S3 in the *Supplementary Materials*), which basically simultaneously satisfies the resolution and control distribution shape distortion (Wu et al., 2018; Fu et al., 2025). Therefore, the MSE indicates the average uncertainty of the riverbed in the tidal channel.

According to the Shannon Entropy (Shannon, 1948), the maximum MSE of the system indicates the state of any discrete source distributed with equal probability, so the Maximum Morphology Shannon Entropy can be defined as:

$$H_m(X) = \log_2 n \tag{6}$$

when n = 40, maximum MSE $Hm(X)$ = 5.322. In addition, the Mean Morphology Shannon Entropy (MMSE) can be defined as

$$\overline{H}(X) = \sum_{i=2}^{n} \frac{1}{i}, \tag{7}$$

when n = 40, $\overline{H}(X)$ = 4.73, which indicate a certain state if H less than $\overline{H}(X)$.

3. Results

3.1. Variations in the shoal-channel system

3.1.1. Changes of the shoal-channel contours

The 2-m isobath effectively delineates the spatial distribution of subtidal shoals, with its temporal variations reflecting bathymetric heterogeneity across the shoal system. From 1955 to 1970, the western 2-m isobath exhibited slight eastward migration, whereas the eastern sector remained relatively stable (Fig. 2a). Between 1970 and 1989, minimal changes were observed except for localized expansion near Haixinsha Island (Fig. 2b). By 2000, the 2-m isobath maintained its eastward advance near Haixinsha Island while exhibiting a distinct westward retreat near Xinsha Port, leading to a pronounced convergence of isobaths in the middle reach of SZY (Fig. 2c). During 2000–2010, the western 2-m isobath continued its eastward displacement while retreating shoreward near Xinsha Port, indicating a narrowing of the tidal channel (Fig. 2d). Post–2010, the 2-m isobath near Xinsha Port vanished, reemerging in the mid-channel with a quasi-elliptical morphology (Fig. 2e). Collectively, these patterns demonstrate a persistent eastward migration of the western 2-m isobath and the development of a quasi-elliptical form in this tide-dominated estuary from 1955 to 2019, ultimately restructuring the shoal configuration of the SZY (Fig. 2f).

The 5-m isobaths are commonly recognized as the boundary between shoals and channels in the estuarine system, and their morphological evolution reflects the marginal dynamics of the tidal channel in the SZY Tidal Channel. Between 1955 and 2019, progressive adjustments along the channel margins were captured by shifting 5-m isobaths (Fig. 3). It could be seen from Fig. 3a that SZY developed a unique shoal-channel structure that maintains a "3-channel-2-shoal" configuration in its middle reaches. During 1955–1970, the 5-m isobaths exhibited eastward migration, with partial disappearance in the eastern segments of both the lower and upper reaches (Fig. 3a). From 1970 to 1989, they stabilized overall but showed a reduction in enclosed areas within the middle

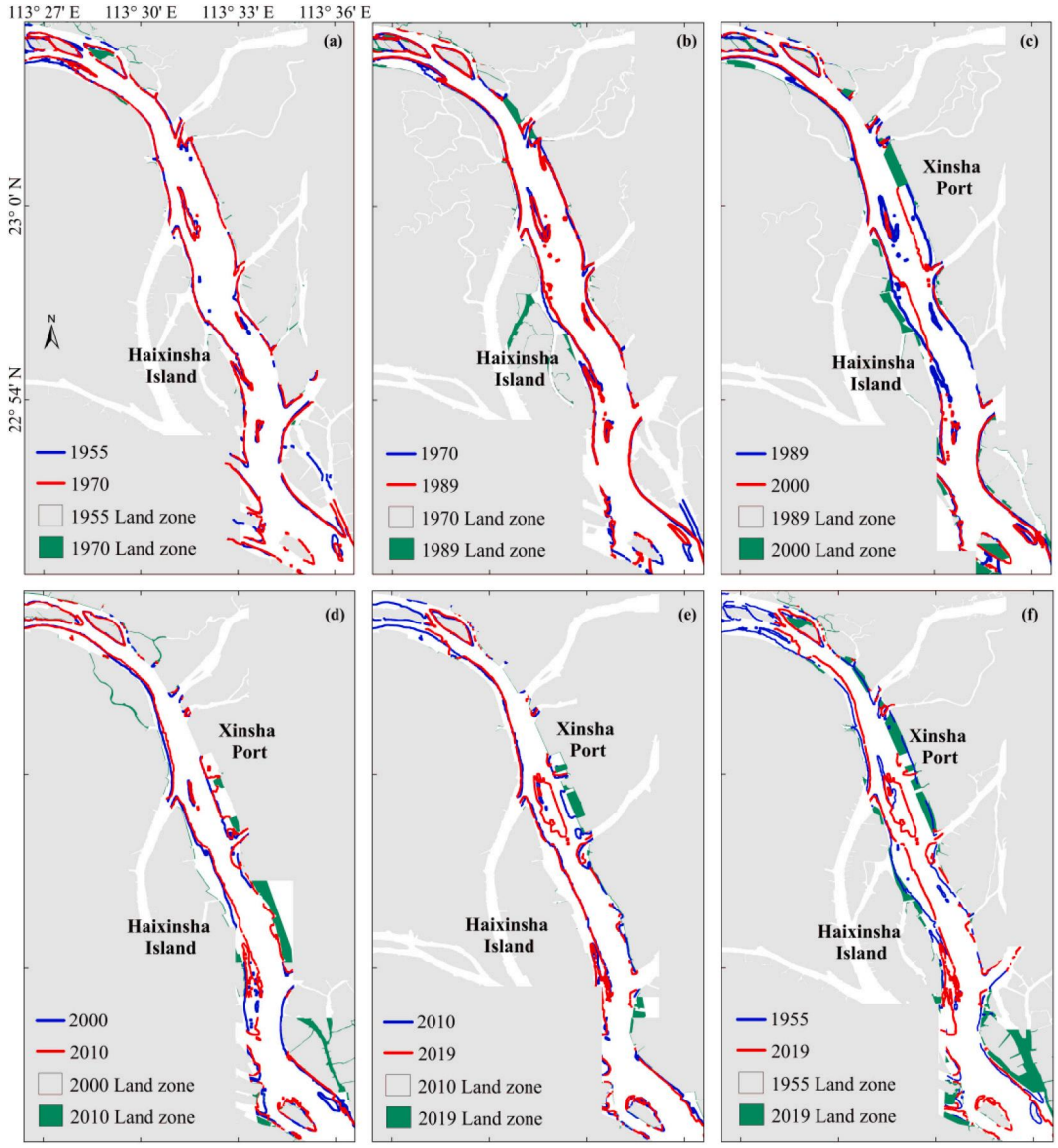

Fig. 2. Changes in the 2-m contour lines of the SZY during 1955–2019.

reach (Fig. 3b). Subsequently, between 1989 and 2000, the 5-m isobaths underwent significant reorganization, vanishing near the lower SZY and Xinsha Port while becoming more pronounced around Haixinsha Island (Fig. 3c), and this eastward migration continued until 2010 (Fig. 3d). Post–2010, the 5-m isobaths largely stabilized, except in the middle reach, where they assumed a quasi-elliptical configuration (Fig. 3e). Collectively, these changes illustrate a transformation from the original "3-channel-2-shoal" to a simplified "2-channel-1-shoal" system from 1955 to 2019, ultimately altering the natural shoal-channel system of the SZY (Fig. 3f).

3.1.2. *Evolution of the shoal-channel*

To characterize the evolution of shoals and troughs in SZY, we employed hypsometric curve analysis to investigate their structural configuration, evolutionary trends, and geomorphological dynamics. The depth-area distribution curves reveal significant temporal variations, with only two distinct peaks observed at 5.50 m and 14.62 m in 1955, while six pronounced peaks emerged at 0.25 m, 1.60 m, 4.89 m, 10.22 m, 12.53 m, and 20.00 m by 2019 (Fig. 4a). The shoal-trough system underwent remarkable geomorphic evolution from 1955 to 2019, marked by an increase in depth peaks from two to six. This tripling of bathymetric features signifies the development of two new shallow shoal formations and two additional deep channel systems throughout the study period.

The corresponding geomorphological units in 1955 and 2019 are presented in Fig. 4c and Fig. 4d, respectively. The characteristic peak depths of 5.50 m (1955) and 4.89 m (2019) represent typical shoal-channel demarcation, while the shallower features at 0.25 m and 1.60 m in 2019 correspond to high-elevation tidal shoals and intertidal zones, respectively. The deeper bathymetric features at 10.22 m, 12.53 m, and 20.00 m in 2019 reflect localized depressions in the seafloor morphology. Notably, the shoal-trough system has transitioned from a relatively simple, naturally dominated configuration to a more complex, multi-factor influenced regime (Fig. 4c-d). The area cumulative frequency analysis (Fig. 4b) further demonstrates that shoal areas (depth $<$ 5 m) have become shallower with the cumulative curve moving leftward from 1955 to 2019, while the trough regions (depth $>$ 5 m) have experienced significant deepening with the cumulative curve moving rightward. The morphological changes have built a compound channel from the relatively simple one, enriching the diversity of shoal-channel structures.

The shoal-channel evolution patterns in the lower, middle, and upper

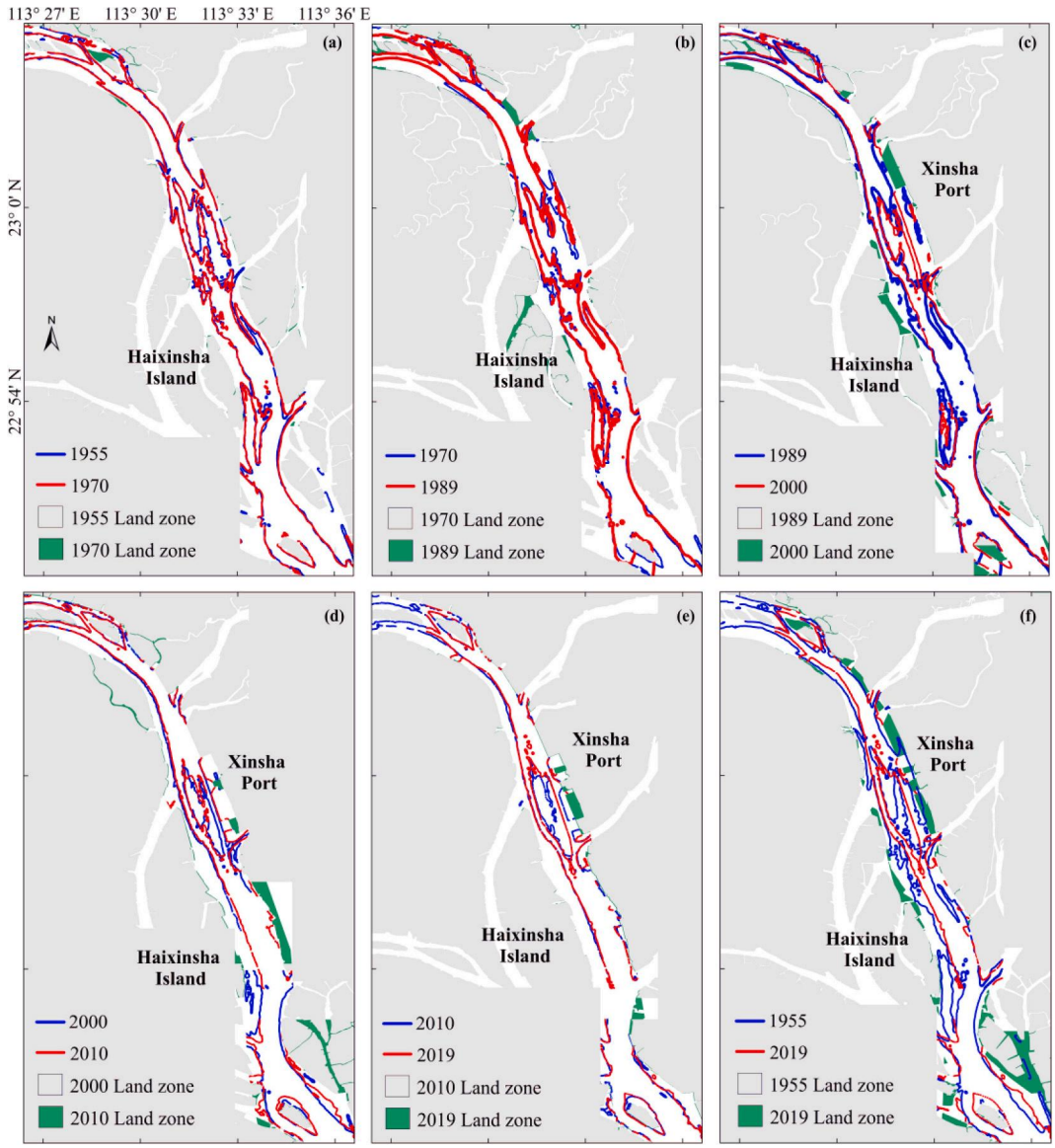

Fig. 3. Changes in the 5-m contour lines of the SZY during 1955–2019.

reaches of SZY were comparatively analyzed between 1955 and 2019 (Fig. 5). The analysis revealed distinct spatial variations: in the upper reach, eastern shoals exhibited significant shrinkage while western shoals expanded progressively, accompanied by eastward migration and elongation of the Huangpu scouring channel (Fig. 5b). The middle reach underwent remarkable geomorphic reorganization, where two discrete shoals merged into a single quasi-elliptical depositional body, leading to channel simplification from three to two distinct pathways with notable deepening of the eastern channel (Fig. 5c). Concurrently, the western shoal demonstrated areal expansion while the eastern sector transformed into a well-defined deep channel, reflecting fundamental shoal-channel transitions in SZY. Like the upper reach, the lower reach displayed western shoal extension coupled with eastern shoal diminishment, along with pronounced upstream extension of the Humen scouring channel (Fig. 5d). Overall, these changes demonstrate a consistent trend of western shoal expansion and eastern shoal contraction throughout SZY from 1955 to 2019, complemented by the progressive development of scouring channels.

3.1.3. Variations of shoal-channel volumes and surface areas

During 1955–2019, the SZY Tidal Channel underwent stepwise variations in water depth: it decreased from 6.35 m to 6.30 m (1955–1970), was followed by a remarkable increase at a rate of 7.80 cm/yr during 1989–2000, and then progressively deepened to 7.53 m (Table 1). Concurrently, total volume initially decreased from 401.12 × 10^6 m^3 to 399.70 × 10^6 m^3 (1955–1989), then increased to 420.53 × 10^6 m^3 in 2010 before stabilizing at 412.62 × 10^6 m^3 in 2019 (Fig. 6a). Furthermore, shoal areas (0–5 m) lost 62.48 × 10^6 m^3 volume (68.88 % to 51.83 % of total) while channel zones (>5 m) gained 73.90 × 10^6 m^3 (31.11 % to 48.17 %) during 1955–2019 (Fig. 6b), achieving near-equilibrium with shoal areas by 2019. Notably, the period 1989–2000 witnessed a pronounced morphological divergence, with the shoal zone (0–5 m) experiencing substantial volumetric loss (−9.21 %) while the channel zone (>5 m) showed commensurate gain. Moreover, surface area declined by 13.18 × 10^4 m^2/yr overall, with shallow areas showing fluctuating decreases from 22.48 × 10^6 m^2 to 21.53 × 10^6 m^2 (Fig. 6c), but increasing proportional coverage (35.57 % to 39.31 %), contrasting with steady deep-zone losses (64.43 % to 60.69 %, see Fig. 6d).

3.2. Stepwise deposition-erosion patterns

Dramatic alterations in erosion and deposition were observed across

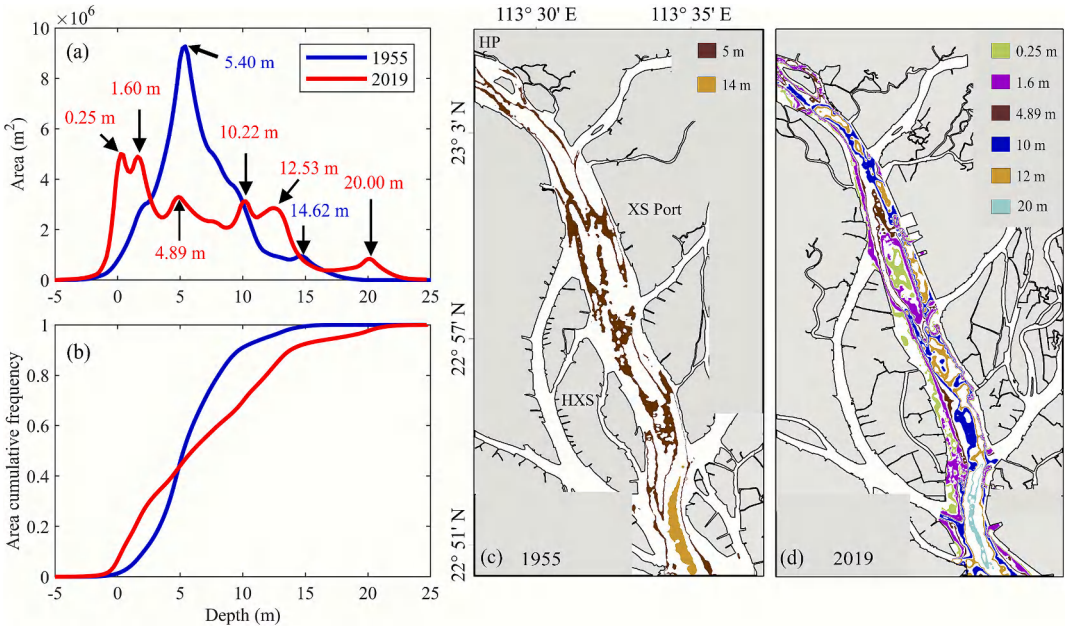

Fig. 4. (a) Depth-area distribution and (b) cumulative frequency curves for the SZY Tidal Channel in 1955 and 2019; (c, d) Corresponding bathymetric maps showing the area between peak depths.

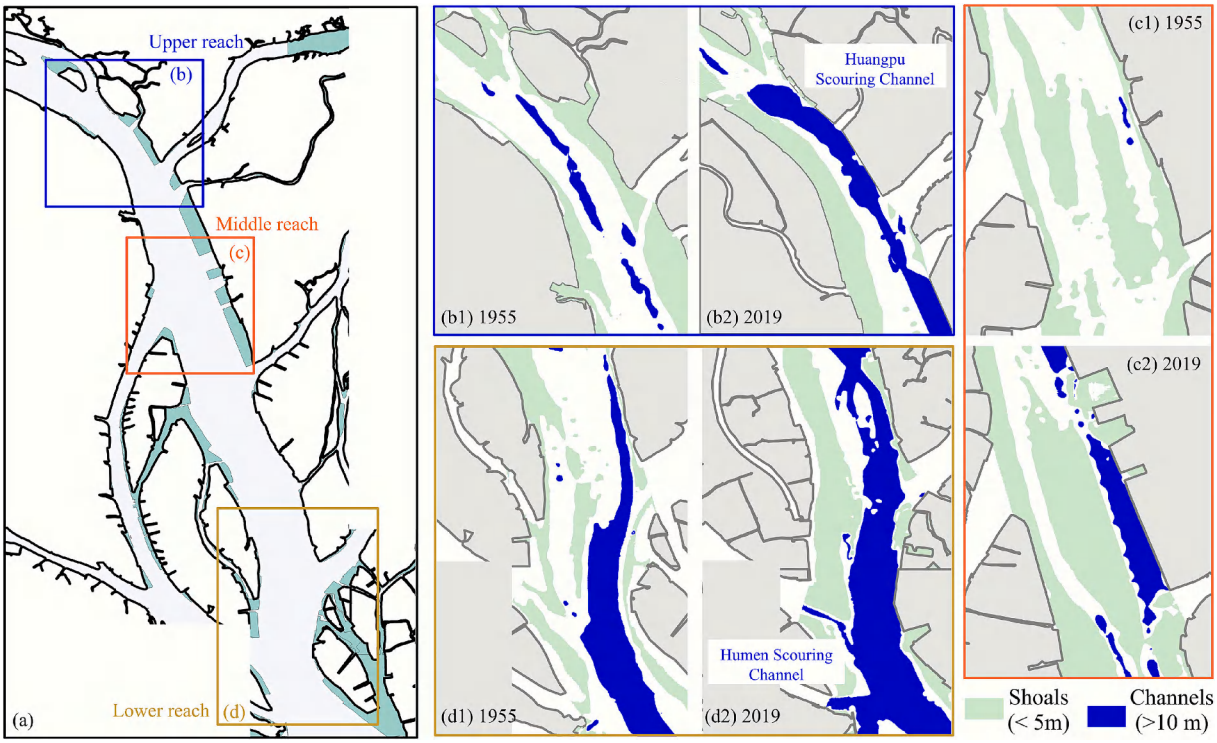

Fig. 5. Evolution of the shoal-channel system in (a) upper, (b) middle, and (c) lower reach of SZY.

Table 1
Variation of mean depth.

Calendar	1955	1970	1989	2000	2010
Mean depth (m)	6.35	6.30	6.43	7.29	7.45

various timescales in SZY over recent decades, with stepwise spatial patterns of deposition and erosion displayed in Fig. S2 (see *Supplementary Materials*). From 1955 to 1970, SZY experienced rapid siltation with a net rate of 0.4×10^6 m^3/yr, driven by a deposition rate of 2.16×10^6 m^3/yr and an erosion rate of 1.76×10^6 m^3/yr (Fig. 7a–b), reflecting a natural tidal-dominated shrinkage phase. This is followed by a period of near equilibrium (1970–1989), with minimal net erosion -0.01×10^6 m^3/yr. A pronounced shift occurred between 1989 and 2000, when erosion intensified to -2.37×10^6 m^3/yr, with erosion exceeding deposition by 1.5-fold. However, this trend reversed post–2000, with net accretion rates of 0.5×10^6 m^3/yr (2000–2010) and 1.0×10^6 m^3/yr (2010–2019).

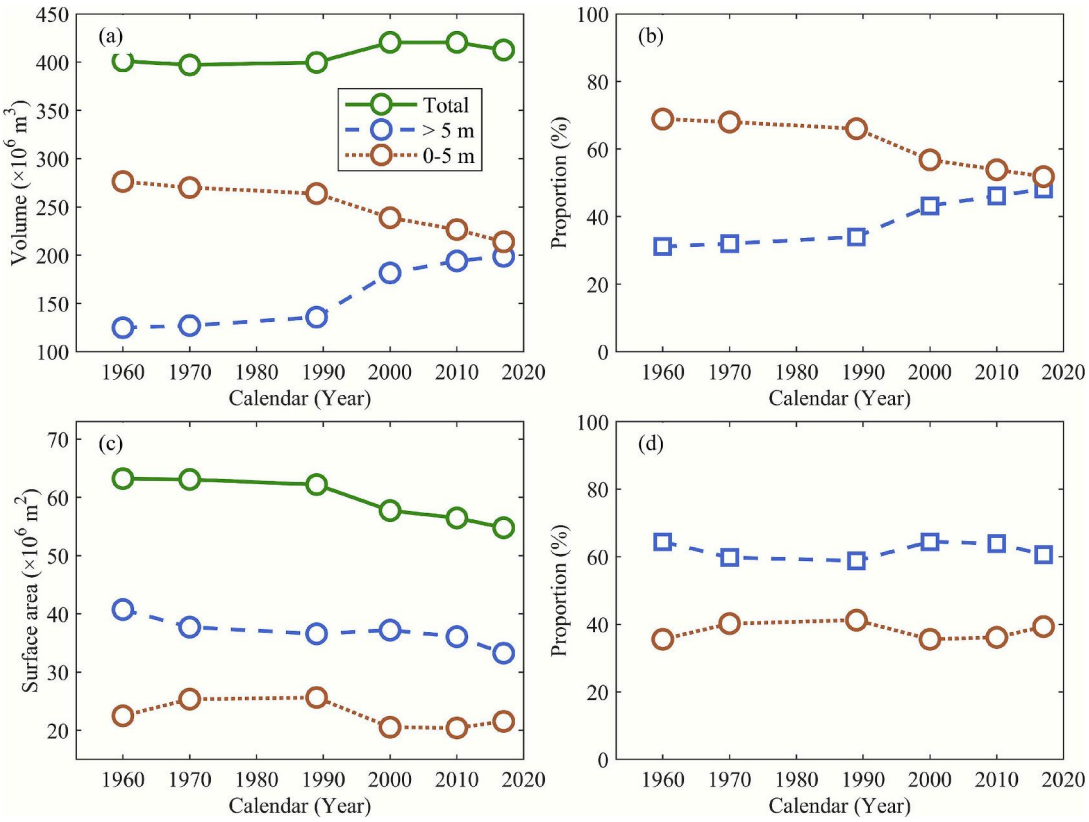

Fig. 6. Temporal variations in volume (a), surface area (b), and their distribution (c, d) during 1955–2019.

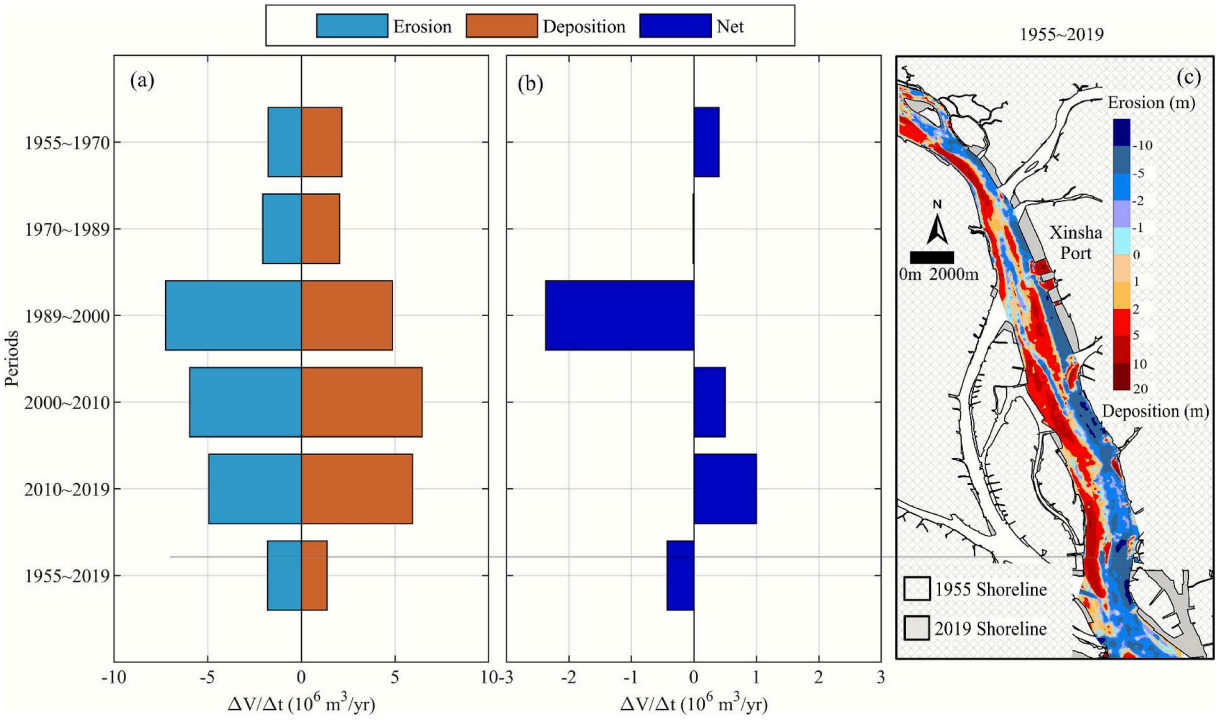

Fig. 7. Volume change rates in the SZY region (1995–2019): (a) erosion-deposition processes, (b) net changes, and (c) spatial patterns.

Cumulatively, the system exhibited a net erosion rate of -0.43×10^6 m^3/yr from 1955 to 2019, spatially characterized by eastern erosion and western deposition (Fig. 7c). A significant geomorphic reorganization occurred in the upper tidal reaches near Xinsha Port, where the deposition-erosion patterns during 1955–2019 drove a remarkable shoal-channel inversion: the former middle channel (Fig. 5c1) accreted to form a shallow shoal (Fig. 5c2), while the original eastern shoal (Fig. 5c1) eroded into a new channel (Fig. 5c2).

3.3. Stability of Shiziyang Tidal Channel

The Morphological Shannon Entropy (MSE) was employed to assess the stability of this tide-dominated estuary, including four typical cross-sections and their spatiotemporal variations. Conceptually, the MSE index measures the "informational complexity" or "disorder" of the seabed's elevation distribution. An increasing trend denotes rising instability and reorganization, while a decreasing trend indicates stabilization and simplification of the seabed form. In addition, the Mean MSE value (black dashed line in Fig. 8b) served as a key metric for quantifying geomorphic complexity and disorder.

In SZY, the MSE increased slightly from 3.87 bits in 1955 to 4.30 bits in 1970, then rose more sharply to 4.51 bits in 1989, peaking at 4.58 bits in 2000 (Fig. 8a), indicating heightened instability during this period. However, it declined to 4.28 bits in 2010 before rebounding slightly to 4.34 bits in 2019, reflecting stepwise shifts in stability. Meanwhile, CS_1 in the lower SZY (Fig. 1) remained stable until its MSE surged from 4.25 bits in 1989 to 4.99 bits in 2010, marking a transition from relative stability to greater complexity. CS_2 exhibited a continuous increase from 4.33 bits in 1970 to 4.98 bits in 2010, followed by a slight decrease to 4.83 bits in 2019, suggesting prolonged instability between 1970 and 2010. In contrast, CS_3 and CS_4 showed no significant long-term trend despite fluctuations from 1955 to 2019, indicating overall stability. Spatially, the MSE variations in SZY revealed stronger disorder in the lower reach (distance <5 km, near Humen Inlet) and upper reach (distance >28 km, near Huangpu), while the section of 22–26 km remained relatively stable (Fig. 8b).

Therefore, a clear four-phase evolutionary progression of the shoal-channel system in the SZY Tidal Channel could be identified by integrating analyses of volumetric changes, surface area variations, accretion and erosion patterns, and MSE dynamics. Specifically, Period I (Pre–1970) maintained natural conditions, Period II (1970–1989) experienced initial anthropogenic disturbances, Period III (1989–2000) underwent the most intensive human modifications, and Period IV (Post–2000) entered an adjustment phase.

4. Discussion

4.1. Anthropogenic interventions

Anthropogenic disturbances have become the primary driver of estuarine bathymetric alterations globally (Hou et al., 2024; Jia et al., 2024; Ralston et al., 2019; Zhong et al., 2024). In this study, we examine the effects of human interventions on the morphological evolution of SZY Tidal Channel through an analysis of satellite-derived land reclamation and port construction patterns (Fig. 9) due to the limitation of bathymetric data. All satellite imagery, specifically, 1989 (Landsat 5 TM), 1993 (Landsat 5 TM), 2006 (Landsat 5 TM), and 2017 (Landsat 8 OLI), underwent radiometric calibration and atmospheric correction to ensure consistency across the multi-temporal dataset. The impact of channel dredging was supported by typical bathymetric cross-sections and the contribution to channel erosion was quantified (Fig. 10).

Satellite imagery analysis reveals significant anthropogenic modification to tidal channel morphology during Period III (1989–2000) and IV (Post–2000), including land reclamation adjacent to Haixinsha Island (Zone S2) and construction of North Xinsha Port (Zone S1), both initiated by July 1989 (Fig. 9a). During Period IV (Post–2000), North Xinsha Port continued through December 2006, ultimately occupying a 583.86 m wide and 1.59 km long footprint (Fig. 9c). Concurrently, South Xinsha Port (Zone S3) underwent construction until 2017, resulting in a width reduction by 20.39 % (622.92 m, Fig. 9c-d). This morphological adjustment correlates with the observed westward migration of the 5 m isobath near Xinsha Port (Fig. 3f). Furthermore, persistent land reclamation near Haixinsha Island (Zone S1) from 1989 to 2017 (Fig. 9a-d) reduced channel width by 455.10 m in the middle reach, coinciding displacement of the 5 m isobath near Haixinsha Island (Fig. 3f). These anthropogenic interventions demonstrate systematic alterations to channel bathymetry through coupled reclamation and port development processes.

The SZY Tidal Channel underwent five distinct dredging phases between 1959 and 2014 (Table 2), which occurred across three periods of stepwise changes of the shoal-channel system. The initial project (PJ-1, 1975–1979) occurred during the Period II (1970–1989) and induced significant western channel deepening (CS_3) from 1970 to 1980 (Fig. 10b). This phase corresponded to an erosion rate of 2.05×10^6 m^3/yr (Fig. 7a) and marked the onset of western cannel erosion during 1970 to 1989 (Fig. S4b in *Supplementary Materials*). Subsequently, the second project PJ-2 (10.5 m depth, 1989 to 1997) shifted the erosion focus on the eastern channel in the upper tidal reach (CS_3) in 2000 (Fig. 10b), generating a peak erosion rate of -7.23×10^6 m^3/yr (Fig. 7a) and further western channel deepening during Period III (1989–2000). Simultaneously, sediment disposal near Xinsha Port triggered substantial localized deposition. Although 2000 bathymetric data are unavailable for the lower reach (CS_1), the third project's (PJ-3: 11.5 m,

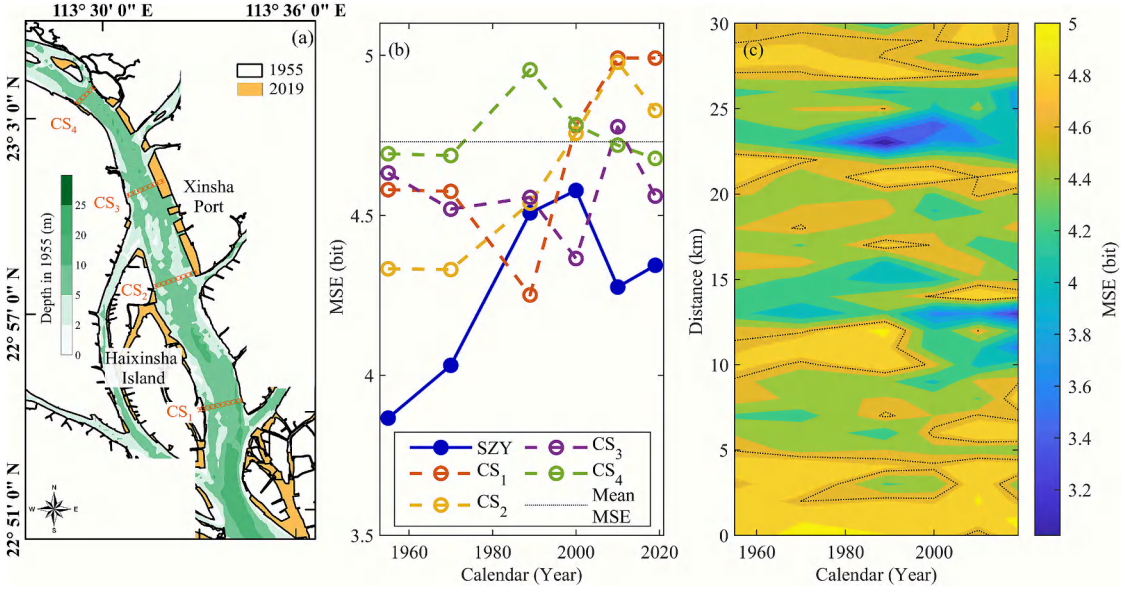

Fig. 8. Spatiotemporal variations of Morphological Shannon Entropy (MSE) in SZY.

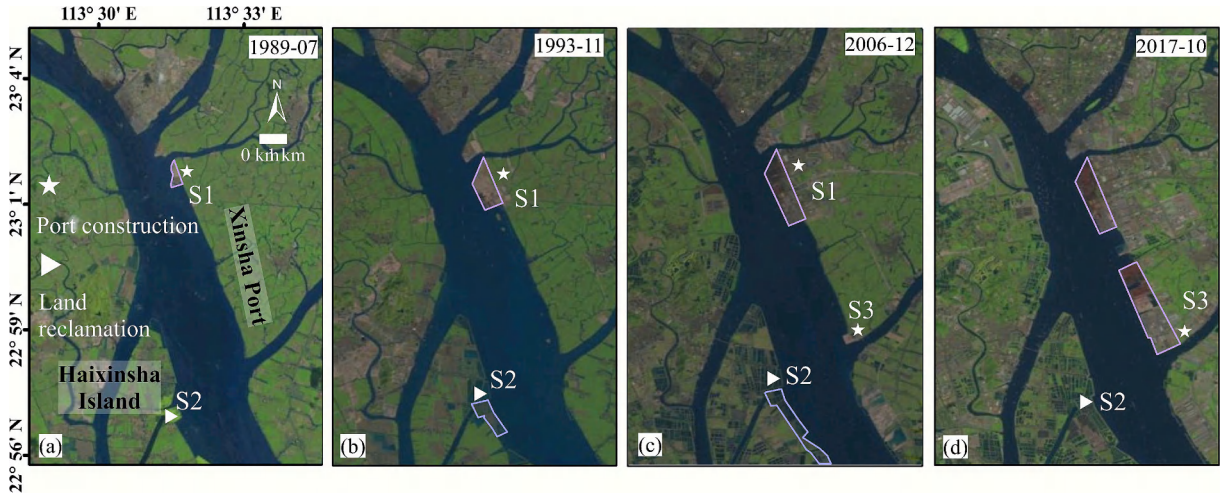

Fig. 9. Landsat images in 1989 (a), 1993 (b), 2006 (c), and 2017 (d) near Xinsha port and Haixinsha island in the upstream of SZY.

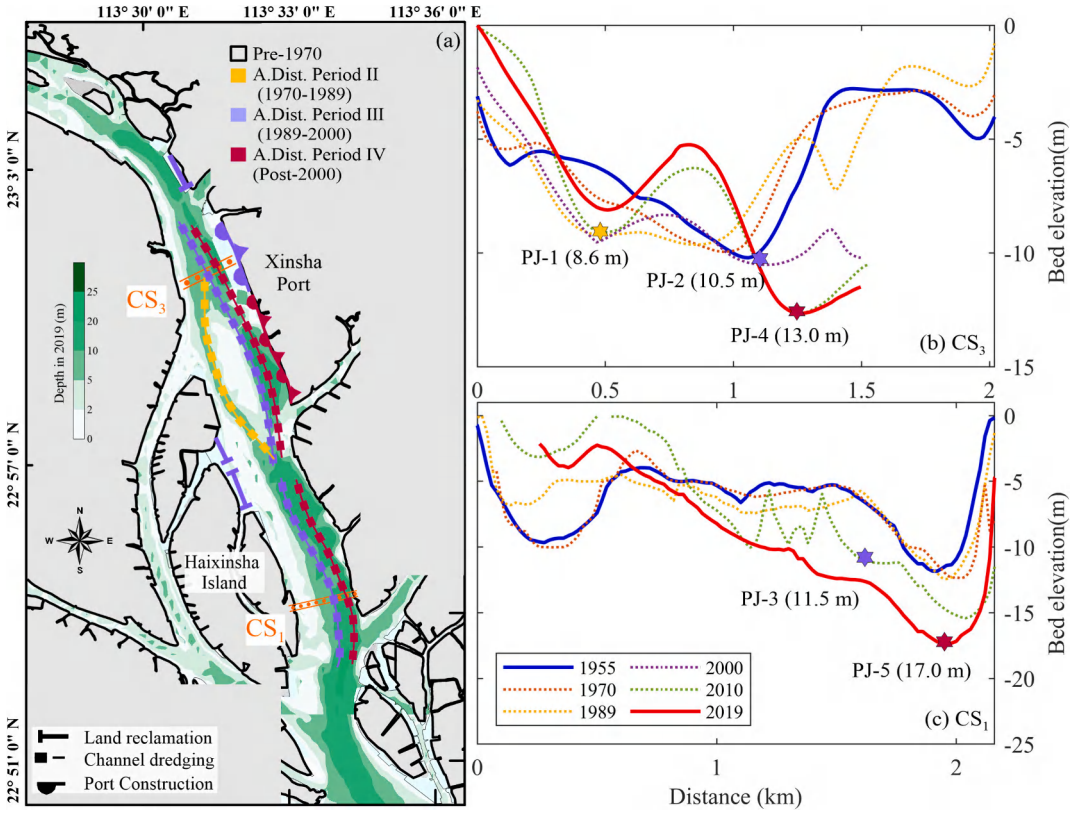

Fig. 10. (a) Spatial pattern of anthropogenic disturbances (A.Dist.), with associated bathymetric evolution shown in the (b) lower and (c) upper characteristic cross-sections.

Table 2
Dredging standards of different projects.

Periods	I	II	III		IV	
Projects	–	PJ-1	PJ-2	PJ-3	PJ-4	PJ-5
Calendar (Year)	–	1975–1979	1989–1997	1998–2000	2004–2006	2011–2014
Dredging depth (m)	–	8.6	10.5	11.5	13.0	17.0

1998–2000) footprint became evident in the eastern lower tidal reach by 2010 (Fig. 10c). Later interventions (PJ-4: 13.0 m depth, 2004–2006) precipitated an eastward migration of the main channel in the upper reach (CS_3, Fig. 10b), while PJ-5 (17.0 m depth, 2011–2014) established persistent deep scour in the eastern lower reach through 2019 (CS_1, Fig. 10c).

To further quantify the contribution of channel dredging, we calculate the ratio of dredging volume to total volume during different periods. Dredging volumes were calculated from bathymetric maps due to a lack of direct project data. Specifically, the dredged area was delineated based on its unique depth profile, and the corresponding volume was then calculated within the identified erosion area (Fig. 11a). Analysis of the attributing ratio in Fig. 11b-c revealed that dredging contributed to 18.63 % (7.25×10^6 m^3 of 38.95×10^6 m^3) of the total scour in Period II (1970–1989). This contribution rose markedly to 68.45 % in Period III (1989–2000), as the dredging volume (54.54×10^6 m^3) constituted the majority of the erosion volume (79.53×10^6 m^3). Subsequently, it declined to an average of 38.45 % in the subsequent period (Post–2000).

4.2. Impacts of fluvial sediment flux

Fluvial sediment supply is fundamental for delta growth, yet the global decline in sediment loads has triggered slower width gain (Liu et al., 2025) and widespread channel erosion (Nienhuis et al., 2020; Wang et al., 2025). Similar to other deltas throughout the world, the SZY Tidal Channel was suffering from reservoir construction in the PRB (Fig. 12a). Between the 1960s and 2010s, the sediment regime was transformed primarily by upstream reservoir construction (e.g., Feilaixia Reservoir on the North River, operational since 1999; Baizhupen Reservoir on the East River, established in 1980) (Liu et al., 2017) and widespread sand mining, which collectively modified the sediment distribution pattern. The changes in sediment distribution and reservoir constructions induced stepwise alteration of sediment flux at Sanshui and Boluo hydrological stations (Fig. 12b). Sediment flux during the flood season from Sanshui station increased from 439.08 kg/s to 660.99 kg/s due to the larger distribution after 1991, but dramatically declined to 436.15 kg/s due to reservoir construction until 2010, followed by a continuous decrease to 238.57 kg/s (Fig. 12c). Concurrently, the sediment flux during the flood season constantly dropped from 144.39 kg/s to 41.28 kg/s (Fig. 12d) in Boluo station.

Sediment inputs from the Pearl River Basin, being redistributed through complex bifurcation networks, exhibit relative influence on the morphodynamics of this tide-dominated channel. The decline in total sediment load led to a pronounced reduction in the shallow-water area (0–5 m depth), particularly affecting the characteristic depositional bank (Fig. 12e) on the western side of SZY (Fig. 12f) between 1955 and 2019. Specifically, the surface area of this depositional bank increased from 0.83 km^2 to 0.97 km^2 during the natural Period I (Pre–1970), primarily due to the sediment supply from the East River. However, it subsequently decreased to 0.44 km^2, plummeting most sharply during Period III (1989–2000) with a 27.65 % reduction, a change attributed to the impact of the Baipenzhu Reservoir construction (Fig. 12g). The loss of shallow area, in turn, facilitated the deepening of adjacent channels, with the increased submerged volume below the 5–m depth (Fig. 6b). It should be noted, however, that this morphological trend was disrupted during the period of high-intensity dredging and disposal (Period III: 1989–2000), when direct anthropogenic activities substantially altered natural sediment dynamics.

4.3. Influences of tidal range and sea level rise

Hydrodynamic forcing, particularly tidal range dynamics and residual water level variations, plays a fundamental role in governing estuarine morphodynamic evolution (Cai et al., 2020; Garel et al., 2021; Mei et al., 2018). As demonstrated by modeling studies in systems such as Victoria, Australia, sea-level rise provides a critical background trend contributing to shoreline recession and morphological adjustment (McCarroll et al., 2025; Thu et al., 2025). Concurrently, hydrodynamic factors play a decisive role in shaping estuarine features, which identifies tidal range as a primary controlling variable for intertidal morphology (Luo et al., 2023; Liu et al., 2025).

While the system's transformation in SZY has been primarily initiated by anthropogenic dredging, these natural forcings can exert a complementary and synergistic influence. The results reveal significant tidal range amplification, with observed increases of 1.77 mm/yr and 4.56 mm/yr at Sishengwei and Huangpu stations, respectively (Fig. 13a). Statistical analyses demonstrate strong positive correlation

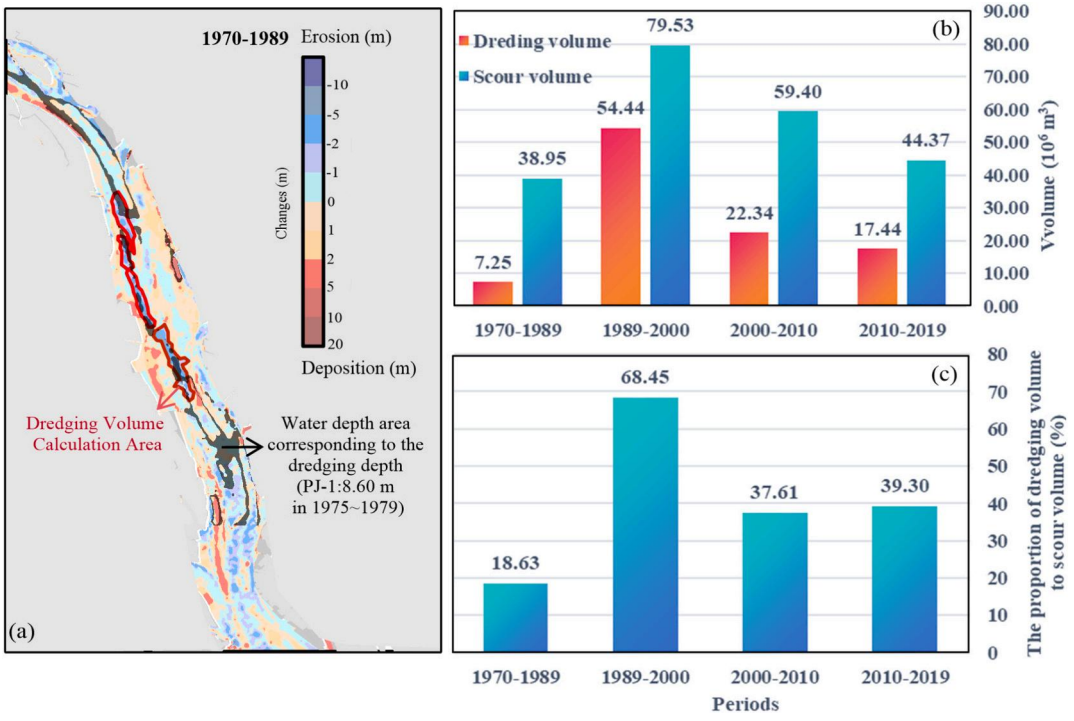

Fig. 11. Illustration of the method for calculating the ratio of dredging volume to scour volume and the results for different periods. (a) An example calculation. (b) Dredging volume and scour volume. (c) Calculated ratios across different periods.

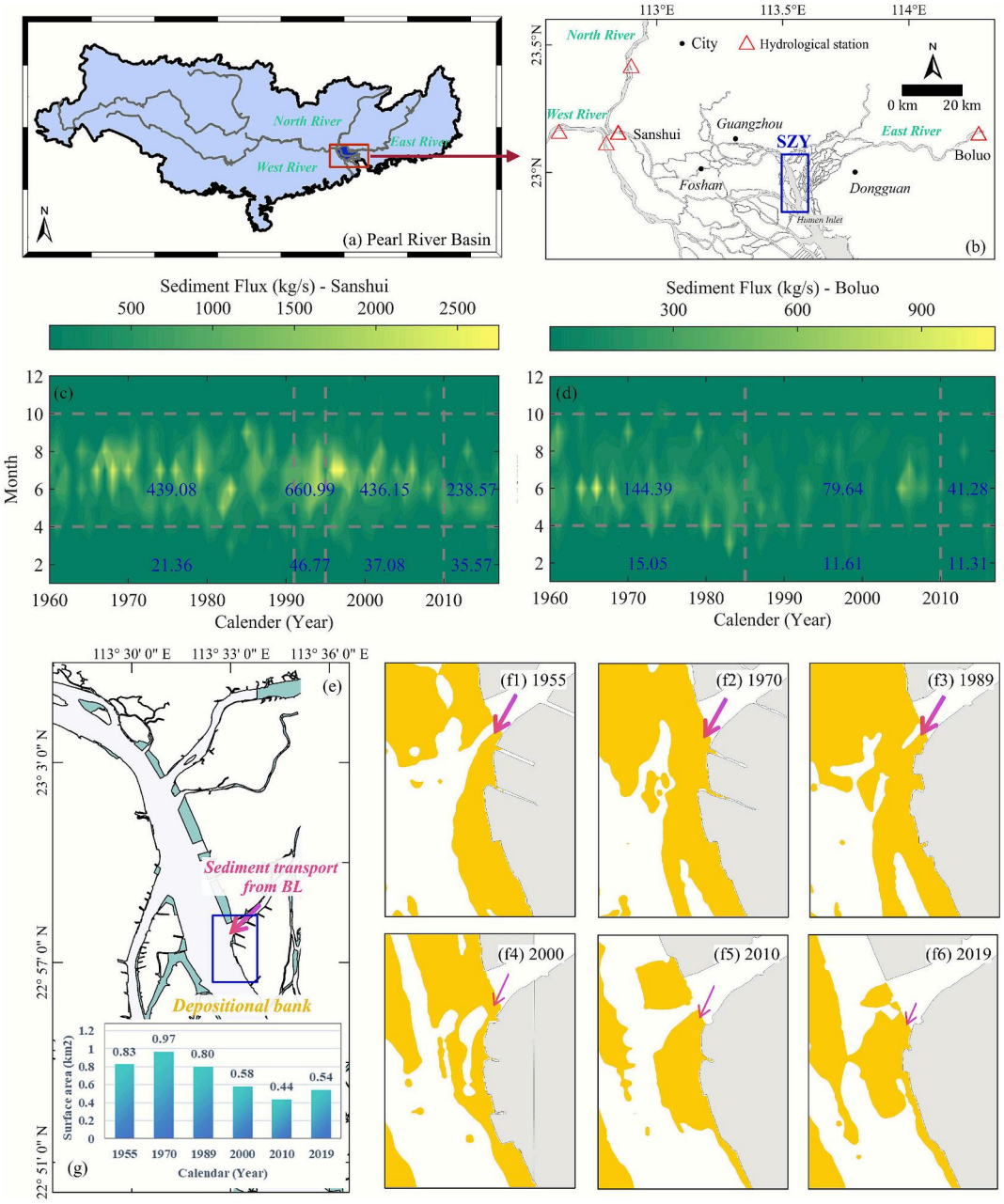

Fig. 12. Geographical locations of Sanshui and Boluo hydrological stations in the Pearl River Basin (a, b), their monthly sediment flux distributions from 1960 to 2019 (c, d). And the spatial variation of a typical depositional bank (e) in SZY (f1-f6) with surface area changes (g) during different periods.

between tidal range enhancement and both mean depth ($R = 0.82$, $p < 0.01$, Fig. 13b) and volume below 5 m ($R = 0.80$, $p < 0.01$, Fig. 13c), except bathymetric data in 2000 that was substantially altered by dredging and its disposal. These relationships indicate tidal amplification likely plays a non-negligible role in driving channel deepening in the SZY.

Additionally, mean sea level trends show comparable rise rates between lower (Sishengwei) and upper (Huangpu) SZY, with an increasing rate of 2.24 mm/yr and 2.33 mm/yr, respectively, indicating the sea level rise in SZY (Fig. 13d). Correlation analyses indicate mean sea level positively correlates with mean depth ($R = 0.85$, $p < 0.01$, Fig. 13e) and channel volume ($R = 0.86$, $p < 0.01$, Fig. 13f), implying sea level rise contributes to channel erosion. The synergistic effects of tidal range amplification and mean sea-level rise have increased bed shear stress in deep channels, leading to enhanced scouring, which is consistent with prior research findings. The presented hydrodynamic results indicate that, alongside the primary driver of channel dredging, the amplification of tidal forces following the deepening has acted as a feedback mechanism, contributing to the subsequent topographic changes. This interplay, though indirect, highlights a complex morphodynamic relationship.

4.4. Schematic map of the evolution of the shoal-channel system

Between 1955 and 2019, the bathymetry configuration of SZY underwent stepwise alterations driven by prolonged anthropogenic disturbances, diminished sediment supply, and eustatic tidal range. During the natural regime Period I (Pre–1970) (Fig. 14a), geomorphology was mainly governed by natural factors, which contributed to shoal accretion (Fig. 5) with a net deposition rate of 1.76×10^6 m^3/yr (Fig. S4a in the *Supplementary Materials*). This phase exhibited a simplistic V-shaped single-channel morphology (Fig. 4c).

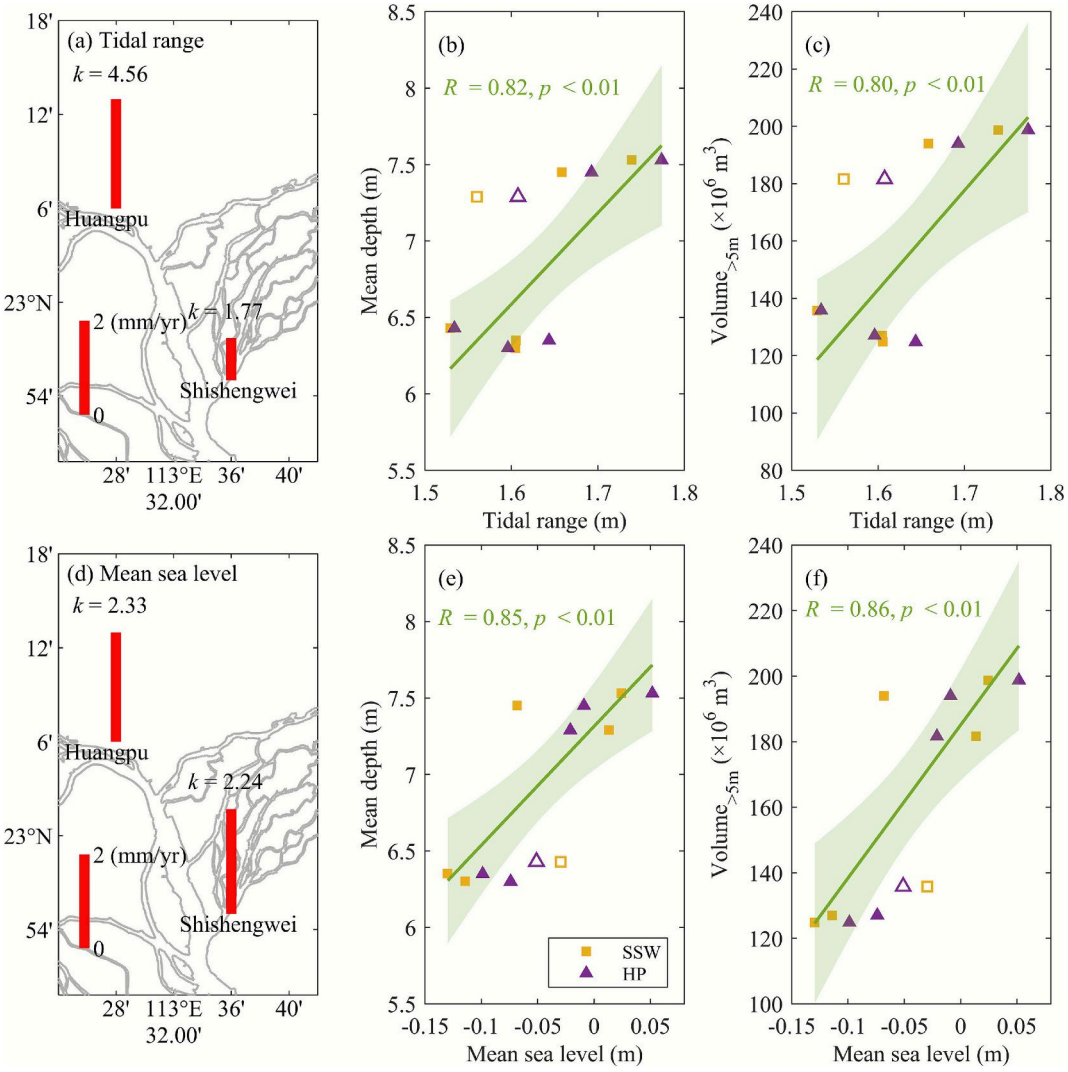

Fig. 13. Long-term (1955–2019) evolution of (a) tidal range and (d) residual water level, and their hydrodynamic coupling with (b, e) volume between 0 and 5 m and (c, f) below 5 m variations.

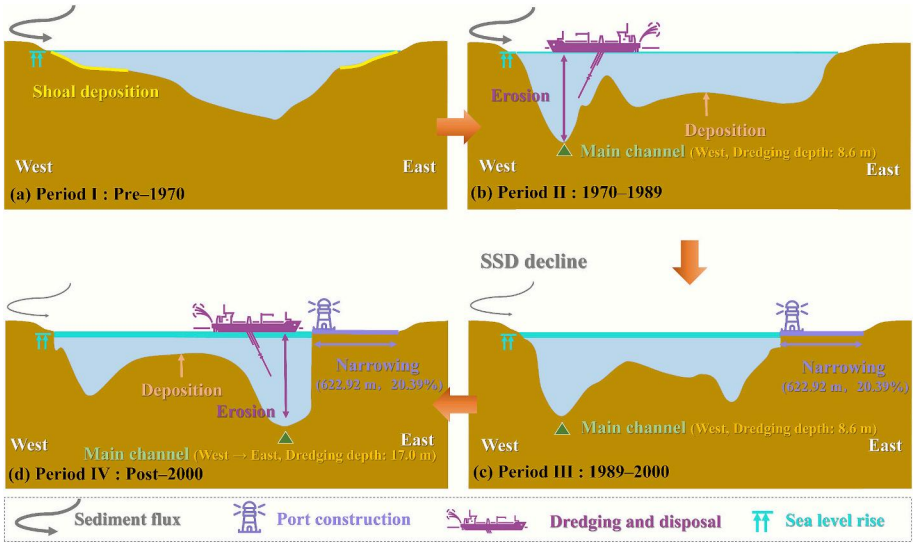

Fig. 14. Schematic diagram of shoal-channel system evolution in SZY during 1955–2019.

Period II (1970–1989) marked the initiation of dredging operations (Fig. 10, Table 2), triggering considerable erosion that carved a deep western navigation channel (Fig. 13b), which subsequently became the main channel in SZY. During this period, a remarkable erosion site could be found in the East Channel near Haixinsha Island (Fig. S4b in the *Supplementary Materials*). The concurrent disposal of dredged material on the eastern side led to the emergence of a W-shaped channel system, with the deeper western channel serving as the primary conduit.

Subsequent intensification of dredging activities focused on the eastern sector (Fig. 14c) during Period III (1989–2000), inducing pronounced channel incisions (Fig. 7a and Fig. S4c in the *Supplementary Materials*) and forming a considerable erosion rate of -7.23×10^6 m^3/yr. This phase coincided with construction at Xinsha Port, which reduced channel width by 20.39 % (Fig. 9). During this phase, SZY experienced the most extensive channel dredging and port construction, which induced a sharp rise in channel volume (Fig. 6b) and net erosion rate of -2.37×10^6 m^3/yr.

The final evolutionary stage (Period IV: 2000–2019) featured continuous eastern channel erosion to 17.0 m depth specifications, affecting a thalweg migration as the eastern channel became hydraulically dominant (Fig. 14d). Strategic placement of dredged material fostered mid-channel shoal development (Fig. 5c), ultimately yielding a dual-channel system flanking a central shoal. Throughout these transformations, synergistic effects of sea-level rise and amplified tidal forcing likely contributed to sustained channel incision within the SZY system.

5. Conclusions

As the essential tidal channel in the PRE, the morphological evolution of the channel-shoal system of SZY has profound implications for water management and navigation. By analyzing the morphological data in the past few decades, we explored the evolution of the shoal-channel system of SZY under the compound factor, and the main conclusions are as follows:

(1) From 1955 to 2019, the deep channel in SZY underwent systematic eastward migration, marked by progressive displacement of the western 2-m isobaths, and the original "3-channel-2-shoal" was remarkably configured into a simplified "2-channel-1-shoal" system. A systematic transformation where substantial volumetric loss (−9.21 %) in shallow shoal areas (0–5 m) was precisely counterbalanced by equivalent accretion in deeper channel zones (>5 m) from 1989 to 2000. This phase coincided with dramatically intensified erosion processes, reaching peak net erosion rates of -2.37×10^6 m^3/yr, which exceeded contemporary deposition by 50 %, collectively driving the system's transition toward its modern configuration.

(2) Stepwise alterations in morphological evolution were detected, with Period I (Pre–1970) characterized by natural conditions, Period II (1970–1989) experiencing initial anthropogenic disturbances, Period III (1989–2000) undergoing the most intensive human modifications, and Period IV (Post–2000) entering an adjustment phase.

(3) Sequential dredging activities (17-m-deep), port construction (20 % width loss), and larger tidal range collectively drove the SZY's transformation from a natural V-shaped single-channel system (Pre–1970) to an engineered dual-channel configuration flanking a central shoal (2000–2019), featuring thalweg migration, hydraulic dominance shifts, and sustained channel incision. Specifically, the period of intensive anthropogenic disturbance (Period III) marked a critical transition of the shoal-channel system in SZY, with the channel dredging corresponding to 68.45 % of the scouring.

CRediT authorship contribution statement

Ping Zhang: Conceptualization, Investigation, Methodology, Writing – original draft. **Linxi Fu:** Methodology, Resources. **Xiangyuan Li:** Investigation, Visualization. **Jianliang Lin:** Funding acquisition, Methodology. **Huayang Cai:** Software, Validation. **Zhijun Dai:** Conceptualization, Funding acquisition, Supervision, Writing – review & editing. **Qingshu Yang:** Conceptualization, Funding acquisition, Supervision.

Declaration of competing interest

The authors declare that they have no known competing financial interests or personal relationships that could have appeared to influence the work reported in this paper.

Acknowledgements

This research was supported by the National Natural Science Foundation of China (NSFC) (Grant No.42430406 and 42406159) and the National Key R&D of China (Grant No.2016YFC0402600).

Appendix A. Supplementary data

Supplementary data to this article can be found online at https://doi.org/10.1016/j.margeo.2025.107694.

Data availability

Datasets related to this article can be available in Mendeley data (https://data.mendeley.com/datasets/py2fhd3fz6/1).

References

Abad, J.D., Garcia, A.P., Marín-Díaz, J., Escobar, C., Ortals, C., Chicchon, H., 2025. Morphodynamics of anabranching structures in the Peruvian Amazon River. Earth Surf. Process. Landf. 50 (1), e6020. https://doi.org/10.1002/esp.6020.

Barua, D.K., 1990. Suspended sediment movement in the estuary of the Ganges-Brahmaputra-Meghna river system. Mar. Geol. 91 (3), 243–253. https://doi.org/10.1016/0025-3227(90)90039-M.

Bilskie, M.V., Hagen, S.C., Alizad, K., Medeiros, S.C., Passeri, D.L., Needham, H.F., Cox, A., 2016. Dynamic simulation and numerical analysis of hurricane storm surge under sea level rise with geomorphologic changes along the northern Gulf of Mexico. Earth's Future 4, 177–193. https://doi.org/10.1002/2015EF000347.

Cai, H., Savenije, H.H.G., Toffolon, M., 2012. A new analytical framework for assessing the effect of sea-level rise and dredging on tidal damping in estuaries. J. Geophys. Res. Oceans 117, C09023. https://doi.org/10.1029/2012jc008000.

Cai, H., Zhang, P., Garel, E., Matte, P., Yang, Q., 2020. A novel approach for the assessment of morphological evolution based on observed water levels in tide-dominated estuaries. Hydrol. Earth Syst. Ences 24, 1871–1889.

Caldwell, R.L., Edmonds, D.A., Baumgardner, S., Paola, C., Roy, S., Nienhuis, J.H., 2019. A global delta dataset and the environmental variables that predict delta formation on marine coastlines. Earth Surf. Dyn. 7, 773–787. https://doi.org/10.5194/esurf-7-773-2019.

Chan, F.K.S., Paszkowski, A., Wang, Z., Lu, X., Mitchell, G., Tran, D.D., Warner, J., Li, J., Chen, Y.D., Li, N., Pal, I., Griffiths, J., Chen, J., Chen, W.-Q., Zhu, Y.-G., 2024. Building resilience in Asian mega-deltas. Nat. Rev. Earth Environ. 5, 522–537. https://doi.org/10.1038/s43017-024-00561-x.

Chen, K., He, Z., Liu, J., Lin, Y., Jia, L., 2022. Long-term morphological evolution and its mechanism of Lingdingyang estuary: interferences from anthropogenic forcings. Mar. Geol. 450, 106856. https://doi.org/10.1016/j.margeo.2022.106856.

Chu, N., Yao, P., Ou, S., Wang, H., Yang, H., Yang, Q., 2022. Response of tidal dynamics to successive land reclamation in the Lingding Bay over the last century. Coast. Eng. 173, 104095. https://doi.org/10.1016/j.coastaleng.2022.104095.

Colina Alonso, A., Van Maren, D.S., Elias, E.P.L., Holthuijsen, S.J., Wang, Z.B., 2021. The contribution of sand and mud to infilling of tidal basins in response to a closure dam. Mar. Geol. 439, 106544. https://doi.org/10.1016/j.margeo.2021.106544.

Dai, Z., 2021. Changjiang Riverine and Estuarine Hydro-Morphodynamic Processes: In the Context of Anthropocene Era. Springer Singapore, Singapore. https://doi.org/10.1007/978-981-16-3771-1.

Dyer, K.R., 1977. Lateral circulation effects in estuaries. In: Estuaries, Geophysics and the Environment. National Academy of Sciences, Washington DC, pp. 22–29.

Fu, L., Zhong, Y., Zhang, P., Niu, L., Zhang, X., Lin, J., Cai, H., Yang, Q., 2025. The evolution and morphodynamic characteristics of shoals and troughs in Lingdingyang Bay of the Pearl River Estuary. Front. Mar. Sci. 12. https://doi.org/10.3389/fmars.2025.1525805.

Galloway, W., 1975. Process framework for describing the morphologic and stratigraphic evolution of deltaic depositional system. In: Soc. Econ. Paleontol. Mineral. SEPM Spec. Publ. No 31, pp. 127–156.
Garel, E., Zhang, P., Cai, H., 2021. Dynamics of fortnightly water level variations along a tide-dominated estuary with negligible river discharge. Ocean Sci. 17, 1605–1621. https://doi.org/10.5194/os-2021-58.
Hoitink, A.J.F., Nittrouer, J.A., Passalacqua, P., Shaw, J.B., Langendoen, E.J., Huismans, Y., van Maren, D.S., 2020. Resilience of river deltas in the anthropocene. Case Rep. Med. 125, e2019JF005201. https://doi.org/10.1029/2019JF005201.
Hou, X., Xie, D., Feng, L., Shen, F., Nienhuis, J.H., 2024. Sustained increase in suspended sediments near global river deltas over the past two decades. Nat. Commun. 15, 3319. https://doi.org/10.1038/s41467-024-47598-6.
Huang, W.P., Hsu, J.C., Ye, C.J., 2023. Assessing the impact factors and corresponding weights affecting the coastal morphology of Hsinchu Coast, Taiwan. J. Sea Res. 195, 102432. https://doi.org/10.1016/j.seares.2023.102432.
Jia, L., Lin, Y., Chen, K., 2024. Long-term morphological evolution and restoration of dredged pits under sand mining in a funnel shaped estuary. Ocean Coast. Manag. 259, 107461. https://doi.org/10.1016/j.ocecoaman.2024.107461.
Kleinhans, M.G., van Scheltinga, R.T., van der Vegt, M., Markies, H., 2015. Turning the tide: growth and dynamics of a tidal basin and inlet in experiments. Case Rep. Med. 120, 95–119. https://doi.org/10.1002/2014JF003127.
Konyssova, G., Sidorenko, V., Androsov, A., Sander, L., Danilov, S., Rubinetti, S., Burchard, H., Winter, C., Wiltshire, K.H., 2025. Changes in tidal dynamics in response to sea level rise in the Sylt-rømø Bight (Wadden Sea). Ocean Dyn. 75, 43. https://doi.org/10.1007/s10236-025-01688-1.
Kuang, C., Liang, H., Gu, J., Song, H., Dong, Z., 2020. Morphological responses of unsheltered channel-shoal system to a major storm: the combined effects of surges, wind-driven currents and waves. Mar. Geol. 427, 106245. https://doi.org/10.1016/j.margeo.2020.106245.
Lin, J., Hu, S., Zhang, P., Fu, L., He, X., Cai, H., Niu, L., Zhang, X., Yang, Q.S., 2025. Spring-neap variations in tidal duration asymmetry in the Pearl River Estuary: dominant tidal combinations and long-term evolution. J. Hydrol. 661, 133684. https://doi.org/10.1016/j.jhydrol.2025.133684.
Liu, F., Hu, S., Guo, X., Luo, X., Cai, H., Yang, Q., 2017. Recent changes in the sediment regime of the Pearl River(South China): Causes and implications for the Pearl River Delta. Hydrol. Process. 32 (12), 1717–1952. https://doi.org/10.1002/hyp.11513.
Liu, S., Hu, Z., Grandjean, T.J., et al., 2025. Dynamics and drivers of tidal flat morphology in China. Nat. Commun. 16, 2153. https://doi.org/10.1038/s41467-025-57525-y.
Luo, J., Dai, Z., Wang, J., Lou, Y., Zhou, X., Tang, R., 2023. Effects of human-induced riverine sediment transfer on deposition–erosion in the South Passage of the Changjiang (Yangtze) delta. J. Hydrol. 622, 129714. https://doi.org/10.1016/j.jhydrol.2023.129714.
Lou, Y., Mei, X., Dai, Z., Wang, J., Wei, W., 2018. Evolution of the mid-channel bars in the middle and lower reaches of the Changjiang (Yangtze) River from 1989 to 2014 based on the Landsat satellite images: impact of the Three Gorges Dam. Environ. Earth Sci. 77, 394. https://doi.org/10.1007/s12665-018-7576-2.
Lou, Y., Dai, Z., He, Y., Mei, X., Wei, W., 2020. Morphodynamic couplings between the Biandan shoal and Xinqiao channel, Changjiang (Yangtze) Estuary. Ocean Coast. Manag. 183, 105036. https://doi.org/10.1016/j.ocecoaman.2019.105036.
McCarroll, R.J., Kennedy, D.M., Ierodiaconou, D., 2025. Morphologically adaptive modelling of sea level rise induced coastal erosion impacts for South-East Australia. Mar. Geol. 488. https://doi.org/10.1016/j.margeo.2025.107602.
Mei, X., Dai, Z., Wei, W., Li, W., Wang, J., Sheng, H., 2018. Secular bathymetric variations of the north channel in the Changjiang (Yangtze) estuary, China, 1880–2013: causes and effects. Geomorphology 303, 30–40. https://doi.org/10.1016/j.geomorph.2017.11.014.
Moore, R.D., Wolf, J., Souza, A.J., Flint, S.S., 2009. Morphological evolution of the Dee Estuary, eastern Irish Sea, UK: a tidal asymmetry approach. Geomorphology 103, 588–596. https://doi.org/10.1016/j.geomorph.2008.08.003.
Nienhuis, J.H., Ashton, A.D., Edmonds, D.A., Hoitink, A.J.F., Kettner, A.J., Rowland, J. C., Törnqvist, T.E., 2020. Global-scale human impact on delta morphology has led to net land area gain. Nature 577, 514–518. https://doi.org/10.1038/s41586-019-1905-9.
Pratolongo, P.D., Perillo, G.M.E., Piccolo, M.C., 2010. Combined effects of waves and plants on a mud deposition event at a mudflat-saltmarsh edge in the Bahía Blanca Estuary. Estuar. Coast. Shelf Sci. 87, 207–212. https://doi.org/10.1016/j.ecss.2009.09.024.
Ralston, D.K., Talke, S., Geyer, W.R., Al-Zubaidi, H.A.M., Sommerfield, C.K., 2019. Bigger tides, less flooding: effects of dredging on barotropic dynamics in a highly modified estuary. J. Geophys. Res. Oceans 124, 196–211. https://doi.org/10.1029/2018JC014313.
Röbke, B.R., Elmilady, H., Chaves, M.A., Taal, M., van der Wegen, M., 2025. The relative impact of sea level rise and dredging strategies on the morphodynamic evolution of the western Scheldt estuary (the Netherlands). Coast. Eng. 200, 104750. https://doi.org/10.1016/j.coastaleng.2025.104750.
Schrijvershof, R., Maren, D.S., Wegen, M., Hoitink, A.J.F., 2024. Land reclamation controls on multi-centennial estuarine evolution. Earth's Future 12 (11). https://doi.org/10.1029/2024EF005080.
Shannon, C.E., 1948. A mathematical theory of communication. Bell Syst. Tech. J. 27, 379–423. https://doi.org/10.1002/j.1538-7305.1948.tb01338.x.
Shimozono, T., Tajima, Y., Akamatsu, S., Matsuba, Y., Kawasaki, A., 2019. Large-scale channel migration in the Sittang River Estuary. Sci. Rep. 9, 9862. https://doi.org/10.1038/s41598-019-46300-x.
Syvitski, J., Saito, Y., 2007. Morphodynamics of deltas under the influence of humans. Glob. Planet. Chang. 57, 261–282. https://doi.org/10.1016/j.gloplacha.2006.12.001.
Talke, S.A., Jay, D.A., 2020. Changing tides: the role of natural and anthropogenic factors. Annu. Rev. Mar. Sci. 12, 121–151. https://doi.org/10.1146/annurev-marine-010419-010727.
Thu, V.T.H., Van Nghi, V., Ngoc, T.A., Hung, T.H., Thai, V.L.D., 2025. Impact of Sea Level Rise and the Superport on Riverbed Morphology in the Can Gio Bay, Southern Vietnam. Thalassas 41, 63. https://doi.org/10.1007/s41208-025-00814-6.
Van Maren, D.S., Beemster, J.G.W., Wang, Z.B., Khan, Z.H., Schrijvershof, R.A., Hoitink, A.J.F., 2023a. Tidal amplification and river capture in response to land reclamation in the Ganges-Brahmaputra Delta. Catena 220, 106651. https://doi.org/10.1016/j.catena.2022.106651.
Van Maren, D.S., Colina Alonso, A., Engels, A., Vandenbruwaene, W., De Vet, P.L.M., Vroom, J., Wang, Z.B., 2023b. Adaptation timescales of estuarine systems to human interventions. Front. Earth Sci. 11, 1111530. https://doi.org/10.3389/feart.2023.1111530.
Wang, H., Zhang, P., Hu, S., Cai, H., Fu, L., Liu, F., Yang, Q., 2020. Tidal regime shift in Lingdingyang Bay, the Pearl River Delta: an identification and assessment of driving factors. Hydrol. Process. 34, 2878–2894. https://doi.org/10.1002/hyp.13773.
Wang, X., Zhang, W., Tong, C., Huang, R., 2024. Unraveling the control factors of long-term morphological evolution in the Yangtze Estuary: a synthesis of natural processes and human interventions. Estuar. Coast. Shelf Sci. 304, 108842. https://doi.org/10.1016/j.ecss.2024.108842.
Wang, J., Dai, Z., Mei, X., Duan, H.-F., Nienhuis, J.H., 2025. Response time of global deltas to changes in fluvial sediment supply. Nat. Commun. 16, 5573. https://doi.org/10.1038/s41467-025-60531-9.
Wu, Z., Milliman, J.D., Zhao, D., Cao, Z., Zhou, J., Zhou, C., 2018. Geomorphologic changes in the lower Pearl River Delta, 1850-2015, largely due to human activity. Geomorphology 314, 42–54. https://doi.org/10.1016/j.geomorph.2018.05.001.
Xie, D., Bing Wang, Z., Huang, J., Zeng, J., 2022. River, tide and morphology interaction in a macro-tidal estuary with active morphological evolutions. Catena 212, 106131. https://doi.org/10.1016/j.catena.2022.106131.
Yang, H., Wang, L., Xu, K., Zhang, W., Shi, B., Yang, S., Wang, Y.P., 2025. Deltaic engineering-induced accumulation hides erosion in response to fluvial sediment decline in the Yangtze submarine shoal. Limnol. Oceanogr. Lett. https://doi.org/10.1002/lol2.70018.
Zeng, W., Dai, Z., Luo, J., Lou, Y., Mei, X., 2024. Morphodynamics of the dredged channel in a mega fluvial-tidal delta. J. Hydrol. 639, 131592. https://doi.org/10.1016/j.jhydrol.2024.131592.
Zhang, W., Cao, Y., Zhu, Y., Zheng, J., Ji, X., Xu, Y., Wu, Y., Hoitink, A.J.F., 2018. Unravelling the causes of tidal asymmetry in deltas. J. Hydrol. 564, 588–604. https://doi.org/10.1016/j.jhydrol.2018.07.023.
Zhang, M., Wu, H., Dai, Z., Mi, J., Cai, H., 2025a. Morphodynamic resilience of the tide-dominated estuary with interference from tidal flat reclamations. J. Geophys. Res. Oceans 128, e2022JC019321. https://doi.org/10.1029/2022JC019321.
Zhang, P., Yang, Q., Liu, H., Dai, Z., Lin, J., Zhang, X., Cai, H., 2025b. Tracking hydrodynamic variation in a tide-dominant estuary over the past half-century. J. Hydrol. 663, 134191. https://doi.org/10.1016/j.jhydrol.2025.134191.
Zhong, Z., Yu, M., Yu, W., Jia, L., Mo, J., 2024. Impact of human-induced alterations in bathymetry and geometry on tidal and salt dynamics: thresholds for morphological dimensions in a convergent estuary. J. Hydrol. 645, 132143. https://doi.org/10.1016/j.jhydrol.2024.132143.
Zhou, Z., Ge, J., van Maren, D.S., Wang, Z.B., Kuai, Y., Ding, P., 2021. Study of sediment transport in a tidal channel-shoal system: lateral effects and slack-water dynamics. J. Geophys. Res. Oceans 126, e2020JC016334. https://doi.org/10.1029/2020JC016334.